Structural and Biochemical Characterization of DHC2, a Novel Diheme Cytochrome *c* from *Geobacter sulfurreducens*[†,‡]

Daniel Heitmann and Oliver Einsle*

Institut für Mikrobiologie und Genetik, Abteilung Molekulare Strukturbiologie, Georg-August-Universität Göttingen, Justus-von-Liebig-Weg 11, 37077 Göttingen, Germany

Received May 27, 2005; Revised Manuscript Received July 18, 2005

ABSTRACT: Multiheme cytochromes *c* constitute a widespread class of proteins with essential functions in electron transfer and enzymatic catalysis. Their functional properties are in part determined by the relative arrangement of multiple heme cofactors, which in many cases have been found to pack in conserved interaction motifs. Understanding the significance of these motifs is crucial for the elucidation of the highly optimized properties of multiheme cytochromes *c*, but their spectroscopic investigation is often hindered by the large number and efficient coupling of the individual centers and the limited availability of recombinant protein material. We have identified a diheme cytochrome *c*, DHC2, from the metal-reducing soil bacterium *Geobacter sulfurreducens* and determined its crystal structure by the method of multiple-wavelength anomalous dispersion (MAD). The two heme groups of DHC2 pack into one of the typical heme interaction motifs observed in larger multiheme cytochromes, but because of the absence of further, interfering cofactors, the properties of this heme packing motif can be conveniently studied in detail. Spectroscopic properties (UV−vis and EPR) of the protein are typical for cytochromes containing low-spin Fe(III) centers with bis-histidinyl coordination. Midpoint potentials for the two heme groups have been determined to be −135 and −289 mV by potentiometric redox titrations. DHC2 has been produced by recombinant expression in *Escherichia coli* using the accessory plasmid pEC86 and is therefore accessible for systematic mutational studies in further investigating the properties of heme packing interactions in cytochromes *c*.

Iron-protoporphyrin IX, or heme, is one of the most widely used prosthetic groups in proteins containing transition metals (*1*, *2*). The largest family of heme proteins, the cytochromes, is named for their deep-red color and fulfils various functions from gas transport to electron transfer and complex enzymatic catalysis. Cytochromes are key players in the electron transport chains of aerobic respiration and photosynthesis in eukaryotes and even more so in most anaerobic metabolisms in prokaryotes. They are further classified according to covalent modifications of the heme cofactor and to its mode of attachment to the protein chain. Unmodified heme groups are found in types *b* and *c*, but while in the former the prosthetic group is only bound by coordination of protein residues to the central iron atom, cytochromes *c* contain additional covalent bonds between the protein and the protoporphyrin moiety (*3*). This attachment of the cofactor typically occurs through the cysteine residues of a conserved binding motif of the C-X_1-X_2-C-H type and the vinyl side chains of the porphyrin (*4*, *5*). It confers additional stability and rigidity to the protein, but requires a complex maturation machinery to attach the heme group to the apoprotein, immediately after its *Sec*-dependent translocation through the cytoplasmic membrane (*6*, *7*). Cytochromes *c* are generally located in "outer" compartments of the cell or organelle, such as the periplasmic space of Gram-negative bacteria or the intermembrane space of mitochondria and chloroplasts in eukaryotic organisms, where they participate in respiratory chains or function as redox enzymes covering a wide range of redox potentials. As a key factor for the protein's functionality, the redox potential of a heme group is fine-tuned by the protein environment, by the nature and orientation of the two axial ligands to the heme iron, and by the ruffling of the porphyrin plane (*8*, *9*). Also, while cytochromes *b* require a large binding pocket for the heme group, *c*-type cytochromes are able to bind numerous cofactors on a short stretch of protein. In such multiheme cytochromes *c*, the heme to protein ratio is high and often only very little protein secondary structure can be observed (*10*). It has also been noted that while multiheme cytochromes *c* do not share sequence homologies to a recognizable degree, they typically do show strong homologies in the arrangement and relative positioning of their heme groups. The cofactors have been found to pack into distinct, recurring motifs, and in particular, two such packing motifs in which two heme groups can pack with their porphyrin planes either in a perpendicular or in a parallel orientation have been identified (*11*, *12*).

In multisite redox enzymes such as hydroxylamine oxidoreductase (HAO)[1] (*13*) or cytochrome *c* nitrite reductase (ccNiR) (*10*, *14*−*16*), several of these motifs are combined to form effective electron transport chains. In HAO, three

[†] This work was supported by Deutsche Forschungsgemeinschaft Grant Ei-520/2 to O.E.

[‡] Structural data have been deposited with the Protein Data Bank as entry 2CZS.

* To whom correspondence should be addressed. Phone: +49 (551) 391 4189. Fax: +49 (551) 391 4082. E-mail: oeinsle@uni-goettingen.de.

10.1021/bi0509999 CCC: $30.25 © 2005 American Chemical Society
Published on Web 08/16/2005

FIGURE 1: Protein sequence of DHC2 from *G. sulfurreducens*, as annotated in the genome (GSU2927) (*21*), and confirmed by the crystal structure. The sequence contains 94 amino acid residues, including a 23-residue signal peptide for periplasmic export. Secondary structures are depicted as derived from the crystal structure. The N-terminal leader peptide sequence is boxed, and helical regions are shown in a symbolic representation. Letters of amino acids not visible in the electron density are shown in gray, and the heme binding motifs are highlighted.

perpendicular packing motifs are joined by two heme groups packing in a parallel motif; in ccNiR, the same interaction occurs for two perpendicular motifs (*10*), and the same scheme is also found in cytochrome c_{554} (*12*), the physiological electron acceptor for HAO. The efficiency of electron transfer in proteins is highly dependent on the distance between centers and their orientation in terms of orbital overlap (*17*), and it can be assumed that within the observed packing motifs these parameters are optimized. In multiheme cytochromes *c*, evolutionary pressure is obviously directed toward keeping these heme-packing motifs intact, and they thus form an essential structural element of the protein, with the consequence that a folded apo form of a multiheme cytochrome *c* does not exist.

Analysis of these proteins is hindered by the fact that the close packing of cofactors results in strong electronic coupling of the metal centers, masking their individual properties. Recombinant production of cytochromes *c* is not straightforward, and consequently, few mutational studies have been carried out on proteins of this class (*18*, *19*).

To study heme interaction in multiheme cytochromes *c* in detail, we sought a protein that (i) is of sufficient simplicity for completely understanding its structural and spectroscopic properties, (ii) can be obtained at good yields by recombinant expression in a standard system such as *Escherichia coli*, and (iii) is relevant for more complex systems as it contains one of the recurring heme-packing motifs. We have characterized a diheme cytochrome *c*, designated DHC2, from the metal-reducing δ-proteobacterium *Geobacter sulfurreducens* (*20*) that fulfils these requirements (Figure 1). The choice of organism was hereby largely based on the fact that the genome of *G. sulfurreducens* contains more than 100 genes for putative *c*-type cytochromes (*21*) and shows a codon usage that very well matches that of *E. coli*. In *G. sulfurreducens*, many of these cytochromes are involved in well-characterized pathways such as nitrate ammonification or novel ones such as dissimilatory metal reduction, but for a majority of these proteins, no function has yet been assigned. DHC2 is an electron transfer protein, one of the smallest of a total of 11 diheme cytochromes encoded in the genome of *G. sulfurreducens*, and its physiological redox partners are unknown. It contains the parallel heme-packing motif and can thus serve as a versatile model system for subsequent mutational studies aimed at developing a better understanding of the properties of heme interaction motifs.

EXPERIMENTAL PROCEDURES

Cloning and Expression of DHC2 in E. coli. Genomic DNA was extracted from *G. sulfurreducens* by standard protocols (*22*) and used as a template for a polymerase chain reaction to amplify the *dhc2* gene (annotated gene GSU2927; http://www.tigr.org). The oligonucleotide primers employed were 5′-G GCC ATG GTC TCC GGT GAA GTA AGG A-3′ and 5′-CC CTC GAG CTT GAA CTT GTG GCA G-3′ for the forward and reverse primer, respectively, where the underlined bases have been modified to introduce restriction sites for endonucleases NcoI and XhoI. The resulting 228 bp product was cloned into a pET-22b(+) expression vector (Novagen) using the same restriction enzymes and transformed into *E. coli* strain XL10-gold. The correctness of the *dhc2*::pET-22b construct was confirmed by sequence analysis. The design of the reverse primer resulted in the omission of the gene's termination codon such that the vector-encoded hexahistidine affinity tag was part of the recombinant protein. The construct was isolated and used for transformation of expression host strain *E. coli* BL21(DE3) that already contained the accessory plasmid pEC86. This plasmid provides the entire cytochrome *c* maturation system (*ccm*) from *E. coli* under the control of a constitutive promoter (*23*). Expression cultures were grown overnight in LB medium at 30 °C without induction.

Protein Purification. E. coli cells were resuspended, homogenized in 20 mM Tris-HCl (pH 7.5), and 150 mM NaCl (purification buffer), and disrupted using an M-110S laboratory microfluidizer (Microfluidics). Cell debris was removed by centrifugation for 15 min at 20000*g*, and the membrane fraction was subsequently separated by ultracentrifugation for 60 min at 4 °C and 100000*g*. The soluble fraction was applied to a nickel-loaded 5 mL Hi-Trap Chelating HP column (Amersham Biosciences). Red protein was eluted with a step gradient of 100 mM imidazole in purification buffer. Fractions containing the cytochrome *c* were concentrated and applied to a Superdex 75 26/60 gel filtration column (Amersham Biosciences) equilibrated with purification buffer without imidazole. For further experiments, the buffer was exchanged for pure H_2O such that the protein could be examined in any desired buffer system. The purity of the eluted cytochrome *c* was confirmed by SDS−PAGE. Protein was determined using the BCA method (*24*).

Spectroscopic Techniques. UV−vis spectra [70 μg/mL protein, in 100 mM HEPES-NaOH (pH 7.5)] were recorded on an Ultrospec 2100 pro instrument (Amersham Biosciences) at room temperature. For the determination of extinction coefficients, protein was lyophilized and weighed out to obtain a solution with a defined protein concentration. EPR spectra of the protein as isolated were recorded in perpendicular X-band mode on a Bruker Elexsys 500 instrument with an ER 049 X microwave bridge (Bruker), equipped with an Oxford Instruments ESR 900 helium cryostat controlled by the ITC 503 temperature device. The modulation frequency was 100 kHz, and the modulation amplitude was typically 0.5 mT. Measurements were per-

[1] Abbreviations: EPR, electron paramagnetic resonance; UV−vis, UV−visible spectroscopy; HAO, hydroxylamine oxidoreductase; ccNiR, cytochrome *c* nitrite reductase; MAD, multiple-wavelength anomalous dispersion; NHE, normal hydrogen electrode.

Table 1: Data Collection Statistics[a]

	remote 1	peak (f′)	inflection (f″)	remote 2
wavelength (Å)	0.9941	1.7394	1.7414	0.9941
resolution range (Å)	50.0−1.6 (1.64−1.60)	50.0−2.25 (2.30−2.25)	50.0−2.25 (2.30−2.25)	50.0−1.5 (1.53−1.50)
no. of reflections	302826	69359	75505	516137
no. of unique reflections	21838	6516	6515	26375
completeness (%)	95.7 (95.9)	81.3 (86.3)	81.2 (83.2)	97.9 (95.1)
$I/\sigma(I)$	10.6 (1.9)	9.0 (6.3)	9.2 (5.6)	10.3 (1.6)
R_{sym}	0.040 (0.47)	0.062 (0.186)	0.046 (0.194)	0.049 (0.559)

[a] The data sets remote 1, peak, and inflection were taken from the same crystal and used for structure solving by MAD. Data set remote 2 was collected from a second crystal and used for refinement. Values in parentheses are given for the highest-resolution shell. R_{sym} is the residual for symmetry-equivalent reflections according to the relation $R_{sym} = \sum_{hkl}[\sum_i|I_{hkl(i)} - \langle I_{hkl}\rangle|/\sum_{hkl}\sum_i I_{hkl(i)}]$.

formed with a Bruker 4122 SHQE cavity at ≈9.38 GHz. The sample tubes were Suprasil quartz tubes (705-PQ-9.50, Wilmad) with an $Ø_{out}$ of 4 mm, and the sample volume was 250 μL. For spin quantitation, a copper standard was measured [anhydrous Cu_2SO_4 in 2 M $NaClO_4$-HCl (pH 1.5)] containing 50 and 200 μM Cu^{2+}, and the results were averaged. The concentration of EPR detectable copper was calculated according to the method of Aasa and Vänngård (*25*), and for quantitation, double-integrated spectra of the reference and sample were compared. Spectra were recorded at different microwave powers to exclude the possibility of saturation.

Redox Titrations. Potentiometric titrations were performed at 298 K in an atmosphere of dinitrogen and monitored using a S2000 fiber optic spectrometer (Ocean Optics) with a deuterium−tungsten halogen light source (Mikropack) following standard protocols. Sodium dithionite (reductant) and potassium hexacyanoferrate(III) (oxidant) were used as described previously (*26*). Samples were buffered with 100 mM HEPES-NaOH (pH 7.5). The amount of reduced DHC2 was calculated by comparing the height of the α-band in different reduction states. During the titrations, small amounts of protein precipitated, which slightly lowered spectroscopic absorption levels. The resulting decrease in the level of absorption was offset by normalizing the spectra with two isosbestic points at wavelengths of 542 and 561 nm, while measuring the peak height at a wavelength of 552 nm. The following mediators were used to a total concentration of 1 μM: methyl viologen (−436 mV), neutral red (−325 mV), safranine (−280 mV), anthraquinone-2-sulfonic acid (−225 mV), 2-hydroxy-1,4-naphthoquinone (−145 mV), phenazine (−125 mV), indigo carmine (−110 mV), resorufin (−51 mV), duroquinone (5 mV), methylene blue (11 mV), juglone (30 mV), 1,4-naphthoquinone (60 mV), *N*-methylphenazonium methyl sulfate (80 mV), and 1,2-naphthoquinone (118 mV). Values in parentheses indicate the respective midpoint potentials. The resulting potentials were recorded using an EMC 50 Ag/AgCl electrode (Sensortechnik, Meinsberg, Germany), which was calibrated with quinone/hydroquinone. All recorded potentials were corrected for the normal hydrogen electrode (NHE).

Crystallization and Data Collection. Purified DHC2 was concentrated to 10 mg/mL and crystallized by the sitting-drop vapor-diffusion method by adding 1 μL of protein solution to 1 μL of reservoir solution and equilibrating against 300 μL of reservoir solution containing 0.2 M $(NH_4)_2SO_4$, 32.5% polyethylene glycol 4000, 0.1 M LiCl, and 0.1 M citrate buffer (pH 3.5). Within 2 days, red crystals appeared at 20 °C. For data collection, crystals were transferred into a cryoprotectant buffer [0.2 M $(NH_4)_2SO_4$, 35% PEG 4000, 0.1 M LiCl, and 0.1 M citrate buffer (pH 3.5)] and flash-cooled in a nitrogen stream. Data sets from this crystal were collected at the EMBL outstation at DESY (Hamburg, Germany) on beamline BW7A. For a multiple-wavelength anomalous diffraction experiment (MAD) (*27*), three data sets were collected from a single crystal, one each to maximize the f' and f'' contributions at the iron K-edge and a third data set at a remote wavelength (Table 1). A second crystal was used to collect high-resolution data for refinement. Data were indexed and integrated using the HKL suite (*28*) (Table 1). The space group was $P2_1$ with the following unit cell constants: $a = 39.64$ Å, $b = 55.67$ Å, $c = 39.63$ Å, and $\beta = 105.91°$. The asymmetric unit contained two protein monomers with a molecular mass of the monomer of 11.31 kDa.

Table 2: Refinement Statistics[a]

no. of protein atoms	1118
no. of heteroatoms	22
no. of heme atoms	172
no. of water molecules	153
R_{cryst}	0.221
R_{free}	0.272
resolution range (Å)	50.0−1.5
mean *B* value (Å^2)	29.3
DPI (R_{cryst}-based) (Å)	0.101
DPI (R_{free}-based) (Å)	0.107
rms deviation from ideality	
bond lengths (Å)	0.014
bond angles (deg)	1.581

[a] DPI is the diffraction precision index introduced by Cruickshank (*59*). rms is the root-mean-square, and residuals are calculated according to the relation $R = \sum_i|F_{obs(i)} - F_{calc(i)}|/\sum_i|F_{obs(i)}|$ for a working set (R_{cryst}) and test set (R_{free}) of reflections.

Structure Determination and Refinement. The four iron atom positions in the asymmetric unit were found using SHELXD (*29*), and subsequent phase calculations and electron density improvement were carried out using SHELXE (*30*). The protein model was built into the resulting, well-defined electron density map using O (*31*) and refined with REFMAC (*32*) against the native, high-resolution data set (Remote2). The model contained 137 amino acids, four heme groups, four sulfate ions, two sodium ions, and 153 water molecules. Refinement was carried out to a total crystallographic *R*-factor of 0.221 and an R_{free} of 0.272 (Table 2). The correctness of the structure was assured with PROCHECK (*32*). A total of 85.7% of the residues occupied the most favored regions and 14.3% of the residues the additional allowed regions on a Ramachandran plot, with no residues in the disallowed regions. Figures representing protein

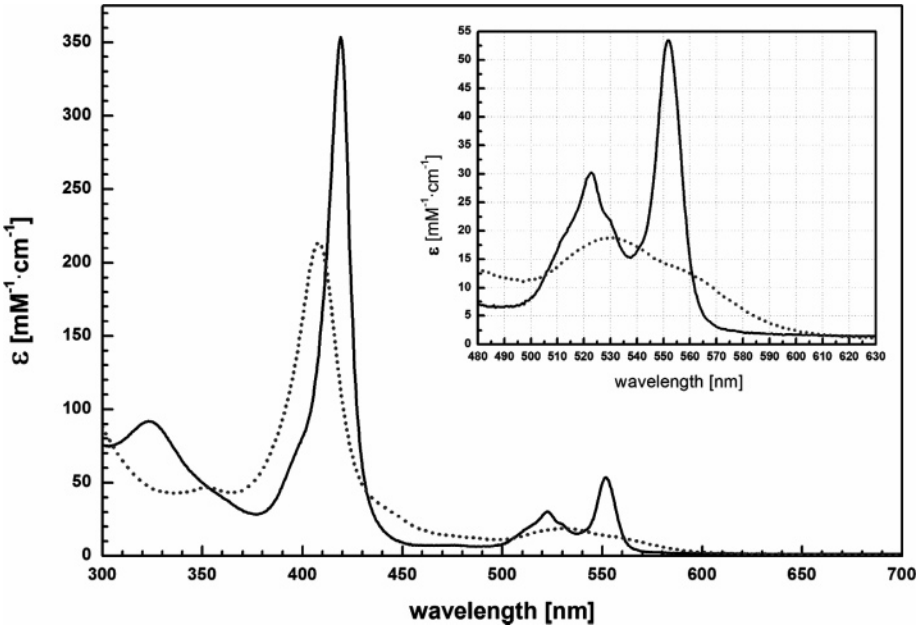

FIGURE 2: Electron excitation spectra of the oxidized (as isolated, ···) and the dithionite-reduced state (—) of DHC2. The oxidized form shows maxima at 408 and 530 nm, whereas the reduced form exhibits a typical, reduced cytochrome *c* spectrum with maxima at 419 nm (γ-band), 523 nm (β-band), and 552 nm (α-band).

structure were made using PyMOL (*33*) and MOLSCRIPT (*34*)/Raster3D (*35*).

RESULTS

Characterization of DHC2. The *dhc2* gene encodes a protein of 94 amino acids, including a cleavable periplasmic export signal comprising residues 1−27 according to the SignalP server 3.0 (*36*). The mature protein therefore consists of 67 residues with a calculated pI of 9.8 and two binding motifs for *c*-type heme groups. Recombinant production of the diheme cytochrome *c* DHC2 in *E. coli* was achieved by coexpression of the *E. coli* cytochrome *c* maturation system from the accessory plasmid pEC86 (*23*). From 6 L of cell culture, ~12 mg of pure protein was obtained and the protein appeared as a single band in silver-stained SDS−polyacrylamide gels. Because of the low abundance of aromatic residues in DHC2, no absorption maximum at 280 nm was visible in UV−vis spectra. The maxima of the spectrum of the oxidized protein were at 408 nm (214 000 M^{-1} cm^{-1}) and 530 nm (18 800 M^{-1} cm^{-1}) (Figure 2). The absence of an additional feature at 610 nm points toward low-spin Fe(III) centers, as it is commonly observed in bis-histidinyl-coordinated cytochromes *c* (*1*, *37*). After reduction with a 10-fold molar excess of sodium dithionite, the protein shows absorption maxima at 419 nm (353 600 M^{-1} cm^{-1}, γ-band), 523 nm (30 200 M^{-1} cm^{-1}, β-band), and 552 nm (53 400 M^{-1} cm^{-1}, α-band), indicating a typical cytochrome *c* spectrum without separable signals from the two individual heme groups. DHC2 can be reduced and oxidized reversibly by several agents (dithionite, Ti(III) citrate vs ferricyanide, dioxygen).

The X-band EPR spectrum of DHC2 exhibits *g* values of 2.96, 2.26, and 1.50 (Figure 3), indicative of low-spin Fe(III) and similar to values obtained with other multiheme *c* systems (*38*), while the additional features at 4.3 and 2.06 may be due to minor impurities of high-spin Fe(III) and Cu(II), respectively. The lines in the spectrum appear to be

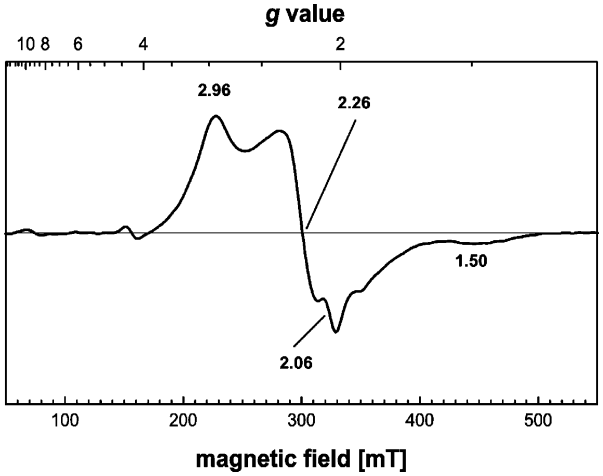

FIGURE 3: EPR spectrum (X-band) of DHC2 at 10 K and a microwave power of 20 mW. The apparent *g* values at 2.96, 2.26, and 1.50 are typical for bis-histidinyl-liganded *c*-type cytochromes with the Fe atoms in a low-spin Fe(III) state, and a small dihedral angle between the histidine imidazole planes. The resonances appear to be slightly broadened, probably the result of magnetic interaction between the iron centers.

relatively broadened, which may be due to coupling of the two heme groups. The low g_{max} value of 2.96 points toward a small dihedral angle for the imidazole planes in the axial coordination positions of both heme groups (*8*). Spin quantitation of the EPR spectrum yielded 2.0 ± 0.2 spins per monomer, indicating that the entire heme content of the protein can be detected.

Redox Titrations. UV−vis-monitored potentiometric titrations of DHC2 showed reversible redox behavior. The redox mediators that were used did not have any significant influence on the absorption behavior of the diheme protein, and titrations were carried out both in the reducing and in the oxidizing direction, yielding identical curves. To model the observed potential curves, two Nernst equations with separately variable midpoint potentials were used (Figure 4). As a further fitting parameter, the relative contribution of

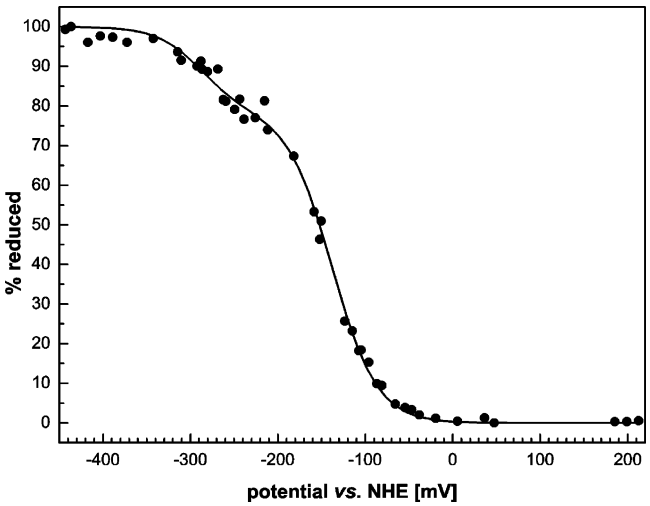

FIGURE 4: Redox titration of *G. sulfurreducens* DHC2 at pH 7.5, monitored at 552 nm. Approximation of the measured points was done by fitting two single-electron Nernst equations with midpoint potentials of −135 and −289 mV with respect to the NHE.

the two heme groups was allowed to vary freely, yielding a ratio of 0.71/0.29. The resulting potentials for the two heme groups of DHC2 were −135 ± 1 and −289 ± 4 mV versus NHE (normal hydrogen electrode) at a buffer pH of 7.5.

Protein Structure and Heme Binding. DHC2 was crystallized in space group $P2_1$ with two monomers per asymmetric unit. These monomers were built and refined separately and included the first residues of the affinity tag, leading to models containing residues 28−97 for monomer A and residues 28−96 for monomer B, with two heme groups in each monomer (Figure 5). Both copies of DHC2 align with a root-mean-square deviation of 0.25 Å for all atoms such that in the following only the monomer will be mentioned. Secondary structures are limited to three α-helical segments. Residues Lys40−Ala47 form helix I; Lys52−Cys59 form helix II, and an additional, short helical segment is located between Cys87 and Cys90. The heme groups are covalently attached to the protein via thioether bonds to cysteine side chains that form part of typical heme binding motifs with the sequence C-X_1-X_2-C-H. The sequence of DHC2 contains two of these motifs, C-V-E-C-H for heme I (Cys59−His63) and C-L-F-C-H for heme II (Cys87−His91). As expected from the observed spectroscopic properties, both axial positions of the heme iron atoms are occupied by histidine side chains, which generally results in a low-spin Fe(III) configuration of the oxidized state. The sixth ligands are His39 for heme I and His76 for heme II. In addition to coordinating the heme iron, the latter seems to be acting as a structural anchor for the N-terminal loop region of DHC2. All four histidines show identical Fe−N_ϵ bond lengths of 2.0 Å at the given resolution of the structure. In heme II, the N_δ atoms of both axial histidines are H-bonded to backbone carbonyl oxygens at a distance of 2.7 Å, while in heme I, the distal His39 forms a longer (2.75 Å) H-bond to the carboxy group of Asp36 and the proximal His63 is bonded to a water molecule at a distance of 2.8 Å.

The second heme binding motif comprises the above-mentioned helical turn, the only secondary structure element in the N-terminal region of the protein. The N- and C-termini of DHC2 are not tightly associated with the rest of the protein and point into the solvent space. Despite the small size of the protein, hydrophobic amino acids Val33, Ala45, Ala50, Phe46, Leu55, Leu88, and Phe93 seem to form a tightly packed folding core. This core region is located between the heme groups and α-helices I and II, and its stability is indicated by *B*-factors well below the overall mean of 29.3 $Å^2$. In addition, residues Val33, Phe42, Ile70, Phe72, and Leu88 show interactions with the hydrophobic porphyrin rings, with approach distances of <3.7 Å. The N-terminal loop region on the opposite site of the heme groups is poorly ordered and shows weaker electron density, which is reflected in increased *B*-factors in the refined structure.

Heme Configuration. The two heme groups of DHC2 (Figure 6) occupy a central position in the protein structure. They are flanked by α-helices I and II on one side and several loop regions at two other sides. The heme iron atoms have a distance of 9.4 Å, whereas the aromatic porphyrin rings approach to a minimum edge-to-edge distance of 4.3 Å. Their porphyrin planes are nearly parallel, but are twisted by 5° around their plane normals, which intersect with a minimum

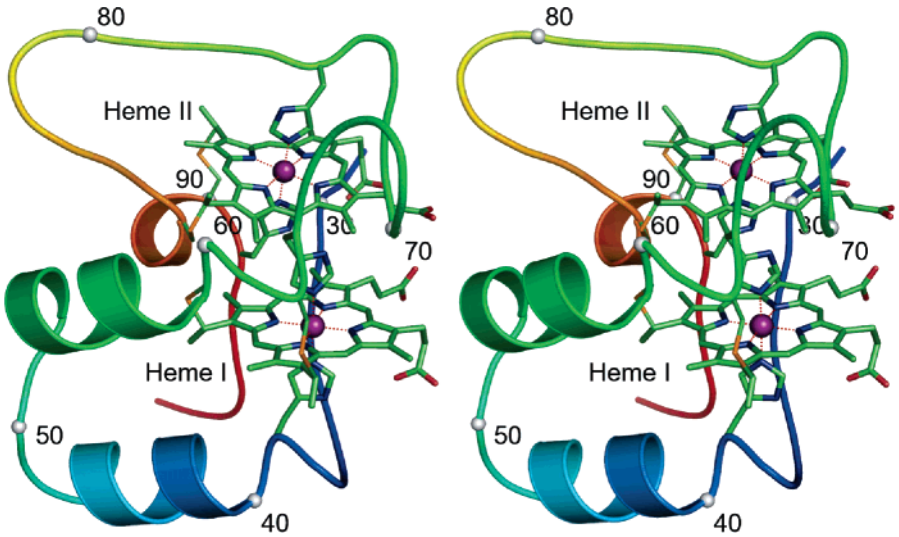

FIGURE 5: Stereoview of the overall structure of *G. sulfurreducens* DHC2. The protein chain is colored continuously from blue at the N-terminus to red at the C-terminus and labeled every tenth residue. The heme groups and their ligands are shown as stick elements and colored by atom type. Purple spheres represent iron atoms.

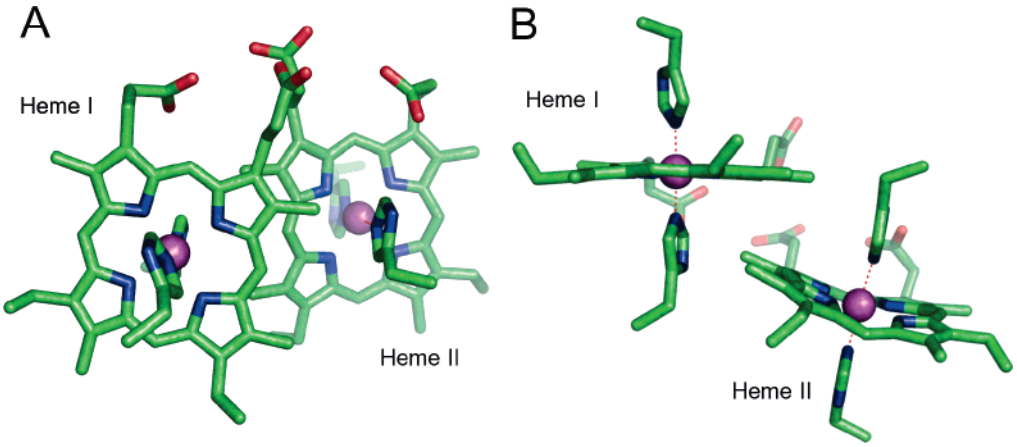

FIGURE 6: Structural arrangement of the heme groups of DHC2. (A) Top view of the nearly parallel porphyrin planes, showing a slight rotation around the *z*-axis (pointing out of the plane of the paper) and a coplanar configuration of the imidazole rings of both histidine ligands of heme II. (B) Side view, showing the planar configuration of porphyrin ring I and the strong distortion of the ruffled porphyrin ring of heme group II.

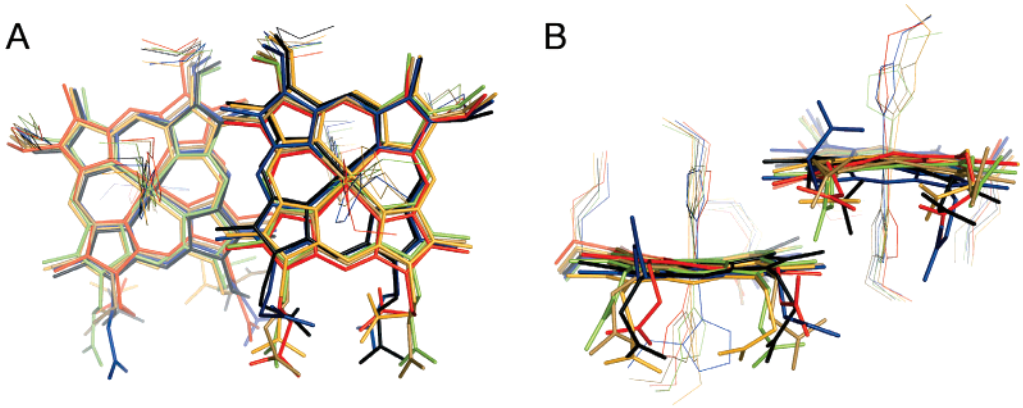

FIGURE 7: Superposition of parallel heme-packing motifs from *G. sulfurreducens* DHC2 (red), *N. europaea* cytochrome c_{554} (blue), *Shewanella putrefaciens* fumarate reductase (brown), *D. desulfuricans* split-Soret cytochrome (black), *H. influenzae* NapB (orange), and *Sulfurospirillum deleyianum* NiR (green). The top view (A) and the side view (B) show that the heme groups are very similar in arrangement and positioning but differ slightly in angles, distances, and porphyrin distortion.

angle of 17°. In the axial histidine ligands of heme group I (His39 and His63), the imidazole planes have an interplanar angle of 36°, whereas those of residues His76 and His91 in heme group II are almost coplanar, with a deviation of only 2°. The porphyrin macrocycle of heme group II is strongly distorted and shows a ruffled configuration, in which the opposing meso-carbon atoms are shifted above and below an imaginary, ideal plane. In contrast, the porphyrin macrocylce of heme group I is almost perfectly planar, with only pyrrole ring B showing a slight out-of-plane arrangement.

Protein Surface. Approximately 87.5% of the surface of DHC2 is formed by amino acids, and 12.5% of the surface consists of heme group atoms. Hereby, heme group I occupies 5.8% and heme group II 6.7% of the total protein surface, mainly by exposing their propionate side chains to the solvent. The total solvent-accessible surface of DHC2 comprises 4201 Å^2. All surface areas were calculated with MSMS (*39*); an electrostatic potential map was calculated with APBS (*40*), and it showed that the charge distribution at the protein surface is not uniform. A negatively charged surface region includes and surrounds the area of the heme propionates, and a positively charged surface area is formed by the N-terminal loop region and the second heme binding motif.

DISCUSSION

The functional properties of the important and widely distributed family of multiheme cytochromes *c* are largely determined by the arrangement and interaction of their multiple heme cofactors. Full understanding of their functional properties will require careful examination of the characteristics of the recurring perpendicular and parallel packing motifs between heme groups, whose exact orientation is conserved to a far higher degree than the sequence and structure of the surrounding protein (*11*). The diheme cytochrome DHC2 (GSU2927) from *G. sulfurreducens* is a novel member of the family of multiheme cytochromes *c*, with no known sequence homologues found in the databases, with the exception of a paralog designated DHC1 (GSU2767) in the same organism. DHC2 is a small, basic protein with two covalently attached heme groups that presumably serves as an electron carrier located in the periplasm of *G. sulfurreducens*. This hypothesis is further supported by the finding that neither DHC1 nor DHC2 is embedded in an operon context with other putative redox-active proteins (*21*).

The heme groups of DHC2 pack into the typical, parallel motif (Figure 7) that has previously been observed in redox proteins as diverse as ccNiRs from various organisms (*10*, *14*−*16*), HAO (*13*) and its physiological redox partner

cytochrome c_{554} from *Nitrosomonas europaea* (*12*), the split-Soret cytochrome *c* from *Desulfovibrio desulfuricans* ATCC 27774 (*41*), flavocytochrome c_3 fumarate reductase (*42*−*44*), and the octaheme tetrathionate reductase from *Shewanella oneidensis* MR-1 (*45*) or the small subunit NapB of the heterodimeric nitrate reductase from *Rhodobacter sphaeroides* (*46*).

All these proteins, however, are not easily accessible through recombinant expression in *E. coli*, or the properties of the heme interaction motif are masked by the presence of a large number of additional heme groups. Only one other reported crystal structure of a diheme cytochrome *c* shows a heme arrangement similar to that of DHC2, namely, the small subunit (NapB) of the periplasmic nitrate reductase from *Haemophilus influenzae* (*47*). With a molecular mass of 14.7 kDa, this protein is similar in size to DHC2, and its two heme groups are arranged in the same parallel packing motif (Figure 7); however, the similarities do not extend to the protein fold beyond the heme-binding sequences themselves. UV−visible spectra of DHC2 are typical for cytochromes *c* (*1*) and do not allow for the distinction of two separate species of hemes. During stepwise oxidation and reduction as carried out during potentiometric analysis, no separate peaks or shoulders have been observed (data not shown). Together with the observed line broadening in the EPR spectrum, this might indicate that the close packing of both hemes, with an iron−iron distance of only 9.4 Å, results in a most efficient coupling of both centers that renders the observation of individual properties impossible. In a potentiometric titration experiment, however, the system will still be able to take up two electrons consecutively, with the observed separated midpoint potentials of −135 and −289 mV. After the first reduction step, the electron would be delocalized between both centers, and this is likely to be functionally relevant for the parallel heme packing motif as a structural module for multiheme cytochromes *c*. Midpoint redox potentials have previously been determined for NapB, yielding values of −25 and −172 mV by cyclic voltammetry for the *H. influenzae* protein (*48*) and −60 and −205 mV by optical redox titration for the protein from *R. sphaeroides* (*46*). Detailed analysis of heme properties has also been carried out for cytochrome c_{554} (*49*, *50*), where the two heme groups packing into a parallel motif have been assigned midpoint potentials of −147 and 47 mV. Despite the highly similar heme arrangement, the span of observed redox potentials is remarkable and reflects the possibilities of fine-tuning through the protein environment that we intend to study in detail using DHC2 as a model system.

As in many other *c*-type cytochromes, the protein part of DHC2 consists exclusively of α-helical secondary structure elements, while the rest of the peptide chain encloses the heme groups in extended loops, leaving them highly exposed to the solvent (*51*). Despite their limited size, α-helices I and II form a stable and rigid core region of the protein that is complemented by the second heme-binding motif (C-L-F-C-H). Both heme groups rest firmly on this part of the protein, and its stability is indicated by low *B*-factors. The distal sides of the heme groups are then only loosely covered by the loop region between residues 64 and 86, reminiscent of the situation observed in the split-Soret cytochrome *c* (*41*). This degree of exposure of the heme groups is likely to facilitate access for the physiological redox partner of the protein. Such features as well as the size of DHC2 support a role either as a soluble, periplasmic electron transfer protein or as a subunit involved in electron transfer within a larger protein complex.

In cytochromes, heme groups are frequently observed to have geometries that deviate from those observed in free solution or many model compounds (*52*, *53*). Such distortions are imposed by the protein, which acts as a complex ligand to finely tune the properties of the metal center (*54*). Apart from hydrogen bonds within the protein, two types of geometric constraints are especially notable, namely, the distortion of the porphyrin plane, termed puckering, and the influence of the relative positioning of the imidazole planes of the two axial histidine ligands (*8*). Both features influence the redox potential of the central iron atom (*55*−*57*), and both are found to varying extents in the heme groups of DHC2.

The histidine ligands of heme group I show an interplanar angle of 36°, while those of heme group II are almost perfectly coplanar. Such small angles in bis-histidinyl-coordinated, low-spin ferricytochromes contribute to regular, rhombic EPR spectra showing maximum *g* values below 3.0, in contrast to larger angles of ∼70° with g_{max} values above 3.0 (so-called "large g_{max}" spectra) (*8*). The observed maximal *g* value of 2.96 therefore already predicted an arrangement such as the one that was subsequently revealed by structural analysis.

The porphyrin macrocycles themselves exhibit different conformations as well. Heme I is almost completely planar, while heme II is strongly distorted into a puckered conformation generally termed ruffled, in which two opposing meso-carbon atoms are located above an ideal plane and the other two below. It has been discussed that ruffling supports a perpendicular arrangement of the imidazole planes of the histidine ligands, in which each of the imidazole rings reaches a maximum distance from the meso-carbon atoms rising above the ideal heme plane on its side (*58*). However, His76 in DHC2 is directly pointing at these atoms, resulting in a conformation that should not be energetically favorable. DHC2 achieves this arrangement by stacking the aromatic imidazole plane between the bulky side chains of Phe72 and Pro77, rendering a rotation into the preferred, perpendicular position impossible. The effect of this strained conformation on the potential and thus the function of DHC2 is not clear, but mutational studies involving the clamping residues will be able to address this question.

With its typical heme packing, DHC2 represents a model system for understanding the function of heme−heme interaction motifs in complex multiheme proteins. In proteins such as ccNiR, HAO, and cytochrome c_{554}, this motif is found to be used as a connection between heme groups showing the perpendicular packing type, and it may indeed be a structural element optimized for efficient electron transfer. To further investigate the properties of the parallel packing motif, mutational studies of DHC2 will be carried out, with the aim of specifically changing functional features such as the axial heme ligands and residues in the immediate surroundings, but also of introducing structural changes on a larger scale that affect the orientation of the heme groups themselves. In every instance, the effect of a mutation on the structure will be confirmed by crystallographic analysis and will be evaluated for changes in spectroscopy and redox

potentials. DHC2 promises to be a suitable candidate for this kind of work, as its overall stability is granted by a rigid folding core that serves as a platform to hold the two heme groups. Leaving this core intact should preserve the structural integrity of the protein, while a multitude of mutations can be used to alter the properties of the heme cofactors themselves.

ACKNOWLEDGMENT

We thank Marc Rudolf and Prof. Peter Kroneck (Universität Konstanz, Konstanz, Germany) for recording EPR spectra of DHC2 and many helpful discussions, Prof. F. Ann Walker (University of Arizona, Tucson, AZ) for critical reading of the manuscript and many valuable suggestions, and Prof. Ralf Ficner for continuous support. The accessory plasmid pEC86 was a generous gift from Prof. Linda Thöny-Meyer (ETH Zürich, Zürich, Switzerland). Synchrotron data were collected at the EMBL BW7A beamline at the DORIS storage ring, DESY.

REFERENCES

1. Pettigrew, G. W., and Moore, G. R. (1987) *Cytochromes c. Biological aspects*, Springer-Verlag KG, Berlin.
2. Moore, G. R., and Pettigrew, G. W. (1990) *Cytochromes c. Evolutionary, structural and physicochemical aspects*, Springer-Verlag KG, Berlin.
3. Thöny-Meyer, L. (1997) Biogenesis of respiratory cytochromes in bacteria, *Microbiol. Mol. Biol. Rev. 61*, 337−376.
4. Stevens, J., Daltrop, O., Allen, J., and Ferguson, S. (2004) C-type cytochrome formation: Chemical and biological enigmas, *Acc. Chem. Res. 37*, 999−1007.
5. Barker, P. D., and Ferguson, S. J. (1999) Still a puzzle: Why is haem covalently attached in *c*-type cytochromes? *Structure 7*, 281−290.
6. Thöny-Meyer, L. (2002) Cytochrome *c* maturation: A complex pathway for a simple task? *Biochem. Soc. Trans. 30*, 633−638.
7. Allen, J., Daltrop, O., Stevens, J., and Ferguson, S. (2003) *C*-type cytochromes: Diverse structures and biogenesis systems pose evolutionary problems, *Philos. Trans. R. Soc. London, Ser. B 358*, 255−266.
8. Walker, F. A. (2004) Models of the bis-histidine-ligated electron-transferring cytochromes. Comparative geometric and electronic structure of low-spin ferro- and ferrihemes, *Chem. Rev. 104*, 589−615.
9. Walker, F. A., Huynh, B. H., Scheidt, W. R., and Osvath, S. R. (1986) Models of the Cytochromes *b*: Effect of Axial Ligand Plane Orientation on the Electron-Paramagnetic-Res and Mössbauer-Spectra of Low-Spin Ferrihemes, *J. Am. Chem. Soc. 108*, 5288−5297.
10. Einsle, O., Stach, P., Messerschmidt, A., Simon, J., Kroger, A., Huber, R., and Kroneck, P. M. H. (2000) Cytochrome *c* nitrite reductase from *Wolinella succinogenes*: Structure at 1.6 Å resolution, inhibitor binding, and heme-packing motifs, *J. Biol. Chem. 275*, 39608−39616.
11. Einsle, O., Messerschmidt, A., Huber, R., Poulos, T., and Wieghardt, K. (2001) *Handbook of Metalloproteins*, Wiley, New York.
12. Iverson, T. M., Arciero, D. M., Hsu, B. T., Logan, M. S. P., Hooper, A. B., and Rees, D. C. (1998) Heme packing motifs revealed by the crystal structure of the tetra-heme cytochrome c_{554} from *Nitrosomonas europaea*, *Nat. Struct. Biol. 5*, 1005−1012.
13. Igarashi, N., Moriyama, H., Fujiwara, T., Fukumori, Y., and Tanaka, N. (1997) The 2.8 Å structure of hydroxylamine oxidoreductase from a nitrifying chemoautotrophic bacterium, *Nitrosomonas europaea*, *Nat. Struct. Biol. 4*, 276−284.
14. Einsle, O., Messerschmidt, A., Stach, P., Bourenkov, G. P., Bartunik, H. D., Huber, R., and Kroneck, P. M. H. (1999) Structure of cytochrome *c* nitrite reductase, *Nature 400*, 476−480.
15. Bamford, V. A., Angove, H. C., Seward, H. E., Thomson, A. J., Cole, J. A., Butt, J. N., Hemmings, A. M., and Richardson, D. J. (2002) Structure and spectroscopy of the periplasmic cytochrome *c* nitrite reductase from *Escherichia coli*, *Biochemistry 41*, 2921−2931.
16. Cunha, C. A., Macieira, S., Dias, J. M., Almeida, G., Goncalves, L. L., Costa, C., Lampreia, J., Huber, R., Moura, J. J. G., Moura, I., and Romao, M. J. (2003) Cytochrome *c* nitrite reductase from *Desulfovibrio desulfuricans* ATCC 27774: The relevance of the two calcium sites in the structure of the catalytic subunit (NrfA), *J. Biol. Chem. 278*, 17455−17465.
17. Page, C. C., Moser, C. C., Chen, X. X., and Dutton, P. L. (1999) Natural engineering principles of electron tunnelling in biological oxidation−reduction, *Nature 402*, 47−52.
18. Wood, L., Muthukrishnan, K., White, T., Ramdas, L., and Nall, B. (1988) Construction and characterization of mutant iso-2-cytochromes-c with replacement of conserved prolines, *Biochemistry 27*, 8554−8561.
19. Mus-Veteau, I., Dolla, A., Guerlesquin, F., Payan, F., Czjzek, M., Haser, R., Bianco, P., Haladjian, J., Rapp-Giles, B., Wall, J., Voordouw, G., and Bruschi, M. (1992) Site-directed mutagenesis of tetraheme cytochrome c_3. Modification of oxidoreduction potentials after heme axial ligand replacement, *J. Biol. Chem. 267*, 16851−16858.
20. Caccavo, F., Lonergan, D. J., Lovley, D. R., Davis, M., Stolz, J. F., and McInerney, M. J. (1994) *Geobacter sulfurreducens sp. nov.*, a hydrogen-oxidizing and acetate-oxidizing dissimilatory metal-reducing microorganism, *Appl. Environ. Microbiol. 60*, 3752−3759.
21. Methé, B. A., Nelson, K. E., Eisen, J. A., Paulsen, I. T., Nelson, W., Heidelberg, J. F., Wu, D., Wu, M., Ward, N., Beanan, M. J., Dodson, R. J., Madupu, R., Brinkac, L. M., Daugherty, S. C., DeBoy, R. T., Durkin, A. S., Gwinn, M., Kolonay, J. F., Sullivan, S. A., Haft, D. H., Selengut, J., Davidsen, T. M., Zafar, N., White, O., Tran, B., Romero, C., Forberger, H. A., Weidman, J., Khouri, H., Feldblyum, T. V., Utterback, T. R., Van Aken, S. E., Lovley, D. R., and Fraser, C. M. (2003) Genome of *Geobacter sulfurreducens*: Metal reduction in subsurface environments, *Science 302*, 1967−1969.
22. Ausubel, F. M., Brent, R., Kingston, R. E., Moore, D. D., Seidman, J. G., Smith, J. A., and Struhl, K. (1990) *Current Protocols in Molecular Biology*, Greene Publishing Associates and Wiley-Interscience, New York.
23. Thöny-Meyer, L., Fischer, F., Kunzler, P., Ritz, D., and Hennecke, H. (1995) *Escherichia coli* genes required for cytochrome *c* maturation, *J. Bacteriol. 177*, 4321−4326.
24. Smith, P. K., Krohn, R. I., Hermanson, G. T., Mallia, A. K., Gartner, F. H., Provenzano, M. D., Fujimoto, E. K., Goeke, N. M., Olson, B. J., and Klenk, D. C. (1985) Measurement of protein using bicinchoninic acid, *Anal. Biochem. 150*, 76−85.
25. Aasa, R., and Vänngård, T. (1975) Signal Intensity and Powder Shapes: A Reexamination, *J. Magn. Reson. 19*, 308−315.
26. Dutton, P. (1978) Redox potentiometry: Determination of midpoint potentials of oxidation−reduction components of biological electron-transfer systems, *Methods Enzymol. 54*, 411−435.
27. Hendrickson, W. A., Smith, J. L., and Sheriff, S. (1985) Direct phase determination based on anomalous scattering, *Methods Enzymol. 115*, 41−55.
28. Otwinowski, Z., and Minor, W. (1997) Processing of X-ray diffraction data collected in oscillation mode, *Methods Enzymol. 276*, 307−326.
29. Schneider, T. R., and Sheldrick, G. M. (2002) Substructure solution with SHELXD, *Acta Crystallogr. D58*, 1772−1779.
30. Sheldrick, G. M. (2002) Macromolecular phasing with SHELXE, *Z. Kristallogr. 217*, 644−650.
31. Jones, T. A., Zou, J. Y., Cowan, S. W., and Kjeldgaard, M. (1991) Improved methods for building protein models in electron-density maps and the location of errors in these models, *Acta Crystallogr. A47*, 110−119.
32. Bailey, S. (1994) The CCP4 Suite: Programs For Protein Crystallography, *Acta Crystallogr. D50*, 760−763.
33. DeLano, W. L. (2002) *PyMol*, DeLano Scientific, San Carlos, CA.
34. Kraulis, P. (1991) Molscript: A program to produce both detailed and schematic plots of protein structures, *J. Appl. Crystallogr. 24*, 946−950.
35. Merritt, E. A., and Bacon, D. J. (1997) Raster3D: Photorealistic Molecular Graphics, *Methods Enzymol. 277*, 505−524.
36. Bendtsen, J., Nielsen, H., von Heijne, G., and Brunak, S. (2004) Improved prediction of signal peptides: SignalP 3.0, *J. Mol. Biol. 340*, 783−795.

37. Gouterman, M. (1978) *The Porphyrins*, Vol. III, Academic Press, New York.
38. Einsle, O., Foerster, S., Mann, K., Fritz, G., Messerschmidt, A., and Kroneck, P. (2001) Spectroscopic investigation and determination of reactivity and structure of the tetraheme cytochrome c_3 from *Desulfovibrio desulfuricans* Essex 6, *Eur. J. Biochem. 268*, 3028−3035.
39. Sanner, M. F., Olson, A. J., and Spehner, J. C. (1996) Reduced surface: An efficient way to compute molecular surfaces, *Biopolymers 38*, 305−320.
40. Baker, N., Sept, D., Joseph, S., Holst, M., and McCammon, J. (2001) Electrostatics of nanosystems: Application to microtubules and the ribosome, *Proc. Natl. Acad. Sci. U.S.A. 98*, 10037−10041.
41. Abreu, I., Lourenco, A., Xavier, A., LeGall, J., Coelho, A., Matias, P., Pinto, D., Carrondo, M., Teixeira, M., and Saraiva, L. (2003) A novel iron centre in the split-Soret cytochrome *c* from *Desulfovibrio desulfuricans* ATCC 27774, *J. Biol. Chem. 8*, 360−370.
42. Leys, D., Tsapin, A. S., Nealson, K. H., Meyer, T. E., Cusanovich, M. A., and Van Beeumen, J. J. (1999) Structure and mechanism of the flavocytochrome *c* fumarate reductase of *Shewanella putrefaciens MR-1*, *Nat. Struct. Biol. 6*, 1113−1117.
43. Bamford, V., Dobbin, P., Richardson, D., and Hemmings, A. (1999) Open conformation of a flavocytochrome c_3 fumarate reductase, *Nat. Struct. Biol. 6*, 1104−1107.
44. Taylor, P., Pealing, S., Reid, G., Chapman, S., and Walkinshaw, M. (1999) Structural and mechanistic mapping of a unique fumarate reductase, *Nat. Struct. Biol. 6*, 1108−1112.
45. Mowat, C. G., Rothery, E., Miles, C. S., McIver, L., Doherty, M. K., Drewette, K., Taylor, P., Walkinshaw, M. D., Chapman, S. K., and Reid, G. A. (2004) Octaheme tetrathionate reductase is a respiratory enzyme with novel heme ligation, *Nat. Struct. Biol. 11*, 1023−1024.
46. Arnoux, P., Sabaty, M., Alric, J., Frangioni, B., Guigliarelli, B., Adriano, J. M., and Pignol, D. (2003) Structural and redox plasticity in the heterodimeric periplasmic nitrate reductase, *Nat. Struct. Biol. 10*, 928−934.
47. Brigé, A., Leys, D., Meyer, T. E., Cusanovich, M. A., and Van Beeumen, J. J. (2002) The 1.25 Å resolution structure of the diheme NapB subunit of soluble nitrate reductase reveals a novel cytochrome *c* fold with a stacked heme arrangement, *Biochemistry 41*, 4827−4836.
48. Brigé, A., Cole, J. A., Hagen, W. R., Guisez, Y., and Van Beeumen, J. J. (2001) Overproduction, purification and novel redox properties of the dihaem cytochrome *c*, NapB, from *Haemophilus influenzae*, *Biochem. J. 356*, 851−858.
49. Arciero, D. M., Collins, M. J., Haladjian, J., Bianco, P., and Hooper, A. B. (1991) Resolution of the 4 Hemes of Cytochrome-c_{554} from *Nitrosomonas europaea* by Redox Potentiometry and Optical Spectroscopy, *Biochemistry 30*, 11459−11465.
50. Upadhyay, A. K., Petasis, D. T., Arciero, D. M., Hooper, A. B., and Hendrich, M. P. (2003) Spectroscopic characterization and assignment of reduction potentials in the tetraheme cytochrome c_{554} from *Nitrosomonas europaea*, *J. Am. Chem. Soc. 125*, 1738−1747.
51. Martin, A., Orengo, C., Hutchinson, E., Jones, S., Karmirantzou, M., Laskowski, R., Mitchell, J., Taroni, C., and Thornton, J. (1998) Protein folds and functions, *Structure 6*, 875−884.
52. Shelnutt, J., Song, X., Ma, J., Jia, S., Jentzen, W., and Medforth, C. (1998) Nonplanar porphyrins and their significance in proteins, *Chem. Soc. Rev. 27*, 31−41.
53. Jentzen, W., Simpson, M., Hobbs, J., Song, X., Ema, T., Nelson, N., Medforth, C., Smith, K., Veyrat, M., Mazzanti, M., Ramasseul, R., Marchon, J., Takeuchi, T., Goddard, W., and Shelnutt, J. (1995) Ruffling in a series of nickel(II) meso-tetrasubstituted porphyrins as a model for the conserved ruffling of the heme of cytochromes *c*, *J. Am. Chem. Soc. 117*, 11085−11097.
54. Ma, J. G., Zhang, J., Franco, R., Jia, S. L., Moura, I., Moura, J. J. G., Kroneck, P. M. H., and Shelnutt, J. A. (1998) The structural origin of nonplanar heme distortions in tetraheme ferricytochromes c_3, *Biochemistry 37*, 12431−12442.
55. Barkigia, K., Chantranupong, L., Smith, K., and Fajer, J. (1988) Structural and theoretical models of photosynthetic chromophores: Implications for redox, light absorption properties and vectorial electron flow, *J. Am. Chem. Soc. 110*, 7566−7567.
56. Ravikanth, M., and Chandrashekar, T. (1995) Nonplanar porphyrins and their biological relevance: Ground and excited-state dynamics, *Coord. Chem. Rev. 82*, 105−188.
57. Kadish, K., Vancaemelbecke, E., Dsouza, F., Medforth, C., Smith, K., Tabard, A., and Guilard, R. (1995) Electrochemistry and spectroelectrochemistry of σ-bonded iron(III) porphyrins with nonplanar porphyrin rings. Reactions of (OETPP)Fe(R) and (OETPP)FeCl, where R = C_6H_5, C_6F_4H, or C_6F_5 and OETPP is the dianion of 2,3,7,8,12,13,17,18-octaethyl-5,10,15,20-tetraphenylporphyrin, *Inorg. Chem. 34*, 2984−2989.
58. Yatsunyk, L., Carducci, M., and Walker, F. (2003) Low-spin ferriheme models of the cytochromes: Correlation of molecular structure with EPR spectral type, *J. Am. Chem. Soc. 125*, 15986−16005.
59. Cruickshank, D. (1999) Remarks about protein structure precision, *Acta Crystallogr. D55*, 1108−1108.

BI0509999